Shape remodeling and blebbing of active cytoskeletal vesicles

Etienne Loiseau, Jochen A. M. Schneider, Felix C. Keber, Carina Pelzl, Gladys Massiera, Guillaume Salbreux, Andreas R. Bausch

BIOPHYSICS

10.1126/sciadv.1500465

Shape remodeling and blebbing of active cytoskeletal vesicles

Etienne Loiseau,[1] Jochen A. M. Schneider,[2] Felix C. Keber,[1] Carina Pelzl,[1] Gladys Massiera,[3] Guillaume Salbreux,[2,4] Andreas R. Bausch[1]*

Morphological transformations of living cells, such as shape adaptation to external stimuli, blebbing, invagination, or tethering, result from an intricate interplay between the plasma membrane and its underlying cytoskeleton, where molecular motors generate forces. Cellular complexity defies a clear identification of the competing processes that lead to such a rich phenomenology. In a synthetic biology approach, designing a cell-like model assembled from a minimal set of purified building blocks would allow the control of all relevant parameters. We reconstruct actomyosin vesicles in which the coupling of the cytoskeleton to the membrane, the topology of the cytoskeletal network, and the contractile activity can all be precisely controlled and tuned. We demonstrate that tension generation of an encapsulated active actomyosin network suffices for global shape transformation of cell-sized lipid vesicles, which are reminiscent of morphological adaptations in living cells. The observed polymorphism of our cell-like model, such as blebbing, tether extrusion, or faceted shapes, can be qualitatively explained by the protein concentration dependencies and a force balance, taking into account the membrane tension, the density of anchoring points between the membrane and the actin network, and the forces exerted by molecular motors in the actin network. The identification of the physical mechanisms for shape transformations of active cytoskeletal vesicles sets a conceptual and quantitative benchmark for the further exploration of the adaptation mechanisms of cells.

INTRODUCTION

Cells need to continuously regulate their shapes to achieve vital processes such as division, motility, or intracellular transport (*1*–*3*). At the microscopic scale, the identification of the mechanisms by which cells achieve such shape changes is hampered by cellular complexity, where a huge number of components interact simultaneously. A minimal model system limited to only a few building blocks would be useful in identifying the physical mechanisms leading to these observed morphologies. Such a synthetic biology approach inspired numerous in vitro studies, ranging from the elasticity of pure lipid vesicles (*4*–*6*), to the dynamics and mechanics of the cytoskeleton (*7*–*9*), to the encapsulation of cytoskeletal components inside vesicles (*10*–*15*). From a mechanistic point of view, all cellular shape changes rely on the composite nature of the involved system: a fluid and easily deformable, but inextensible membrane is tightly coupled to a relatively rigid cytoskeleton that not only provides mechanostability against shear forces to the cell but also actively deforms because of the presence of active motors (*16*–*22*).

Membrane deformations beyond the well-studied equilibrium shapes observed in passive vesicles (*4*–*6*) are only possible in composite systems, where membrane tension and local force production, or reorganization of the cytoskeleton is directly coupled to the membrane. Experiments linking the lipid membrane to a cytoskeletal network located outside the vesicle lead either to a rupture of the cortex, followed by shrinkage around the vesicle, or to a complete crushing of the vesicle (*15*). In this configuration, contractility of the actin network results in a compressive force on the membrane.

Having a tension-generating network inside the vesicle should fundamentally change the situation. Stresses generated in the network result in inward pulling forces acting on the membrane, leading to an increase in membrane surface tension and, because of the law of Laplace, to an internal hydrostatic excess pressure. Such an internal overpressure tends to push water outside the vesicle; however, osmotic pressure also constrains the volume of the vesicle, such that the vesicle does not collapse, and the difference in osmotic and hydrostatic pressure across the membrane balances each other at equilibrium. The tension generated under this set of conditions should now be able to remodel the shape of the vesicles. Such an internal excess pressure is thought to underlie the phenomenon of blebbing (*23*) in living cells, yet a direct evidence for the mechanism can only be achieved with a bottom-up approach using purified components (*24*).

RESULTS

Control of actin network formation in passive cytoskeletal vesicles

Here, we present a minimal model system of a cytoskeletal vesicle by encapsulating actin filaments and the cross-linking protein anillin into vesicles using a modified emulsion transfer technique, continuous droplet interface crossing encapsulation (cDICE) (*25*, *26*). To obtain stable and spherical vesicles, we adjusted the inner and outer osmotic pressures, such that the reduced volume, defined by the ratio between the volume of liquid present in the vesicle and the volume enclosed by a sphere of the same surface area as the vesicle, is only slightly lower than 1. Attachment of the actin network (10 μM) to the membrane is controlled by varying the concentrations of anillin, which has a His tag, as well as of the Ni-NTA (nitrilotriacetic acid) lipids in the lipid membrane (Fig. 1; control experiments in the absence of Ni-NTA are shown in fig. S1). In cells, anillin plays a major role during cytokinesis by maintaining the stability of the cell. Thereby, anillin cross-links the actin while linking the actomyosin network to the cell membrane via a phosphatidylinositol

[1]Department of Physics, Technische Universität München, 85748 Garching, Germany. [2]Max Planck Institute for the Physics of Complex Systems, 01187 Dresden, Germany. [3]Université de Montpellier, Laboratoire Charles Coulomb, UMR 5221, CNRS, F-34095 Montpellier, France. [4]The Francis Crick Institute, Lincoln's Inn Fields Laboratories, London WC2A 3LY, UK.
*Corresponding author. E-mail: abausch@mytum.de

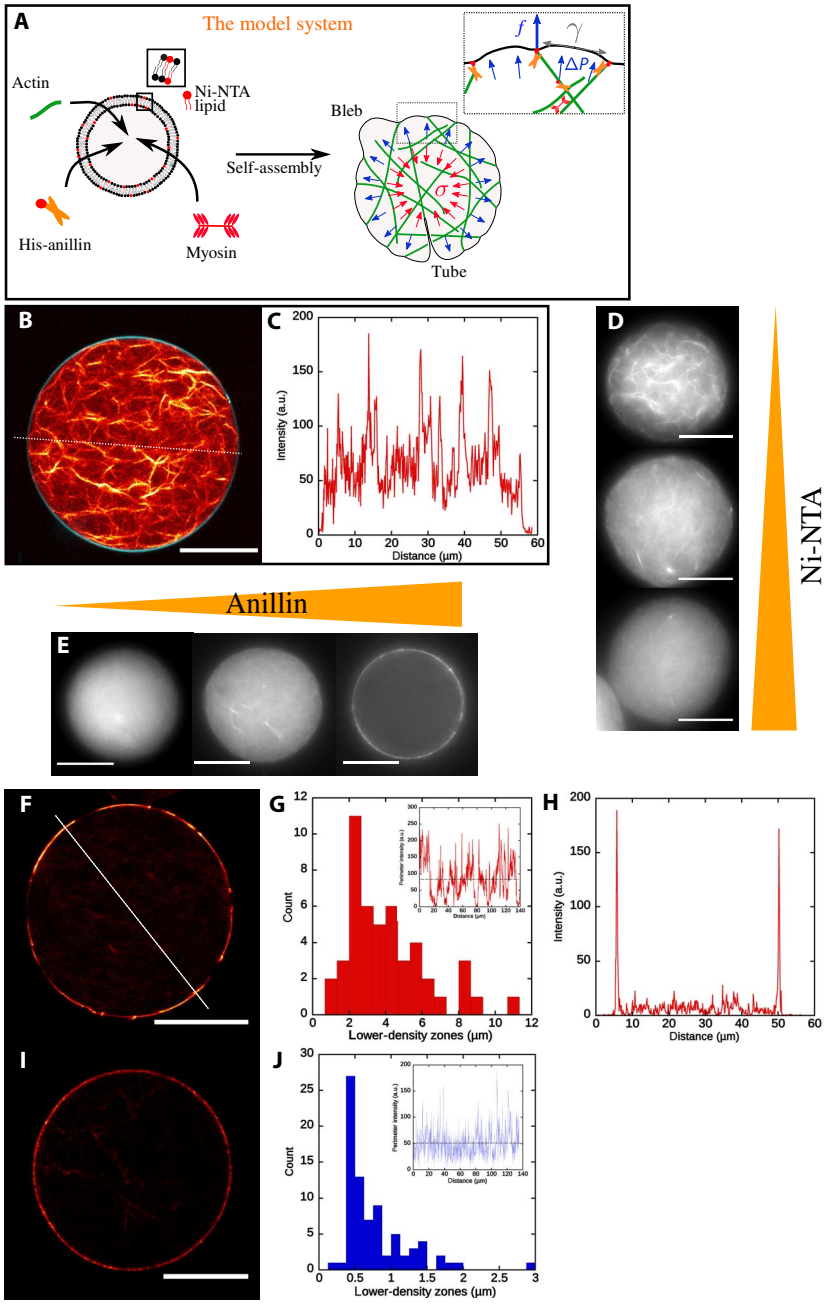

Fig. 1. Reconstruction of a cytoskeleton inside vesicles. (**A**) The lipid membrane contains a fraction of functionalized lipid with a Ni-NTA group. Elementary building blocks encapsulated in the vesicle consist of actin, a polyhistidine-tagged anillin cross-linker, and myosin II molecular motors. The self-organization of these bricks results in the formation of an active cytoskeletal network coupled to the lipid membrane. In the network, the myosin produces a stress σ, which is transduced to the membrane via the Ni-NTA lipid/His-anillin links. Pulling on the membrane leads to the generation of an internal overpressure, Δp, and, hence, an increase of the membrane tension. (**B**) Three-dimensional network coupled to the membrane (10 μM actin, 0.5 μM anillin, and 0.1% Ni-NTA lipid). (**C**) Intensity profile of the actin network along one diameter of the vesicle [dashed line in (B)]. a.u., arbitrary units. (**D**) Increasing the Ni-NTA from 0.1% to successively 1 and 10% favors the recruitment of anillin at the membrane. The bulk is depleted in anillin, which leads to thinner bundles. (**E**) At 10% Ni-NTA lipids, increasing the anillin concentration from 0.1 to 0.5 and 1 μM leads to a transition from a 3D network (0.1 and 0.5 μM) to a 2D cortex-like cytoskeleton (1 μM). (**F**) A 2D cortex-like structure is obtained for 10 μM actin, 1 μM anillin, and 10% Ni-NTA lipid. A confocal picture of the equatorial plane is shown. (**G**) Size distribution of the areas with a lower membrane/cortex anchoring. The size of the areas with a fluorescence intensity lower than the average intensity is extracted from the actin intensity profile plotted along the circumference of the cortex. An example of such a profile is given in the inset. (**H**) The intensity profile of the actin along one diameter [dashed line in (F)] of the vesicle. The two peaks show that actin is recruited at the membrane to form a 2D cortex, but some cytoskeletal material remains in the bulk of the vesicle. (**I**) Vesicle with a 2D cortex, 10 μM actin, 1.5 μM anillin, and 10% Ni-NTA lipid. (**J**) Heterogeneities in the cortex are characterized the same way as in (G). The higher anillin concentration favors the recruitment of actin at the membrane, and the heterogeneities are smaller. Scale bars, 20 μm.

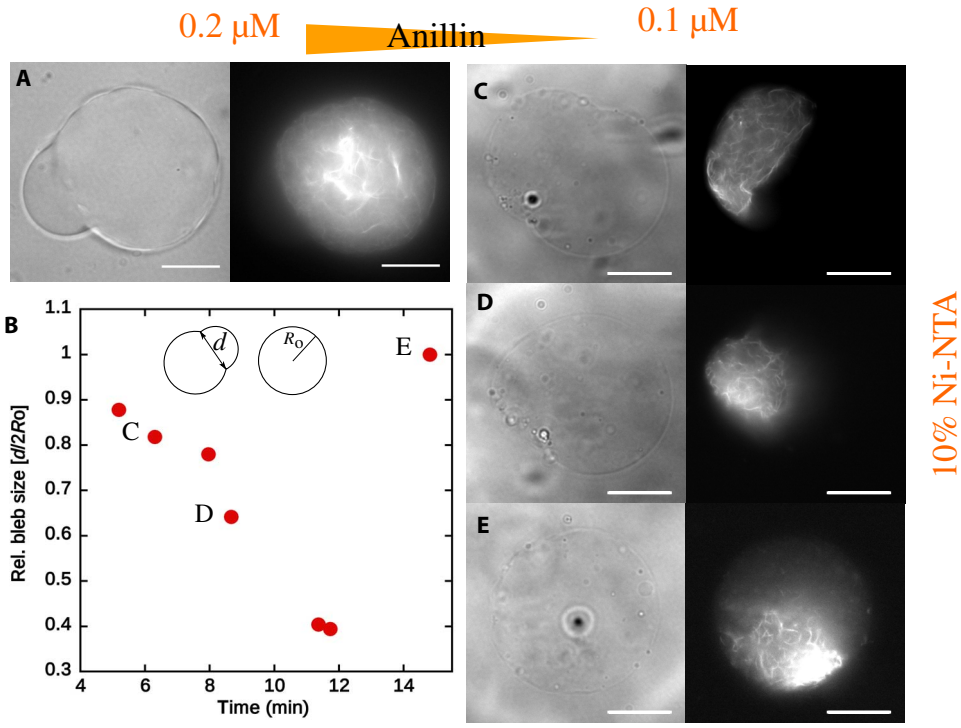

Fig. 2. Stability of single-bleb vesicles containing 1 μM myosin. (**A**) At an anillin/myosin concentration of 0.2:1, we observe the formation of a single bleb that remains stable overtime. The internal overpressure is not strong enough to globally disrupt the coupling to the membrane. (**B** to **E**) Upon decreasing the number of membrane/cytoskeleton links (0.1:1, anillin/myosin), the contraction of the actomyosin network decreases the neck of the bleb (B) and the membrane/cytoskeleton links rupture until the vesicle recovers a spherical shape (C to E). Scale bars, 20 μm. *d*, diameter of the bleb; R_0, radius of the spherical vesicle.

4,5-bisphosphate lipid interaction (*27*). Using the cDICE method to produce these biomimetic vesicles allows an efficient encapsulation of the cytoskeletal proteins and a robust reproducibility (*25*). In a typical experiment, we consider about 75% of the produced vesicles for the analysis. The remaining 25% of the vesicles result from the characteristic polydispersity of the method. The analyzed vesicles remain stable for over a day, at least. For a given set of experimental conditions, at least 40 vesicles with homogeneous morphology were analyzed.

At a concentration of 0.1% Ni-NTA lipids, we observe a volume-spanning actin network inside the vesicles anchored to the membrane via the Ni-NTA–anillin (0.5 μM) interaction (Fig. 1, B and C). Increasing the Ni-NTA lipid concentration to 1% results in a significantly less-bundled network that still spans the entire volume of the vesicle (Fig. 1D). A further increase of the Ni-NTA lipid concentration up to 10% results in even thinner filaments in the volume of the vesicle, yet a cortex remains to be formed. This shows that a higher ratio of Ni-NTA lipids significantly favors the recruitment of the anillin to the membrane but is not sufficient for cortex formation. This suggests that the concentration of cross-linking molecules is the limiting factor for cortex formation. At 0.5 μM anillin, a large fraction of anillin is already bound to the membrane when polymerization and cross-linking of the actin network occur, which depletes anillin from the volume and thus reduces the bundling effect in the vesicle.

Indeed, by increasing the anillin concentration by a factor of 2, we can produce a cortex network tightly coupled to the membrane when 10% Ni-NTA lipids are present (Fig. 1E). Both a high ratio of Ni-NTA lipid (10%) and a high concentration of anillin (1 μM) are required to obtain a two-dimensional (2D) cortex-like structure. Cortex formation was not achieved at a low Ni-NTA concentration of 0.1%, even after a 10-fold higher concentration of anillin was added. Actin is recruited at the membrane, as can be seen on the actin intensity profile along the diameter of a vesicle (Fig. 1H). The fraction of cortical actin depends on the anillin concentration and can be determined by computing the cortex/bulk ratio of actin fluorescence intensity. At 1 μM anillin, cortical actin accounts for 40 to 50% of the total actin. An increase of anillin concentration to 1.5 μM favors the recruitment of cortical actin up to 75%. The cortex has intrinsic heterogeneities consisting of areas of lower cortical actin, as can be observed in Fig. 1 (F and I). We characterized these heterogeneities in the case of two different anillin concentrations by measuring the size of the areas that have an actin fluorescence intensity below the mean intensity. The size distributions are reported in Fig. 1 (G and J). At 1 μM anillin, the low-intensity cortical actin areas range from 2 to 6 μm, whereas at 1.5 μM, the size of the heterogeneities drops to ~0.5 μm. This is consistent with the increase of the fraction of cortical actin previously calculated.

Switching the network geometry from a 3D network (Fig. 1B) to a 2D cortex-like structure (Fig. 1F) does not result in change of the overall vesicle shape; in all cases, the vesicles remain spherical. The fraction of bound anillin can be determined by labeling anillin with Alexa Fluor 488. By computing the ratio of intensities in the volume of the vesicle with the circumference, the absolute bound anillin concentration was determined (see figs. S2 to S4 and the Supplementary Materials for detailed calculations). By this means, the distances between the attachment points are determined and reported in the final phase diagram.

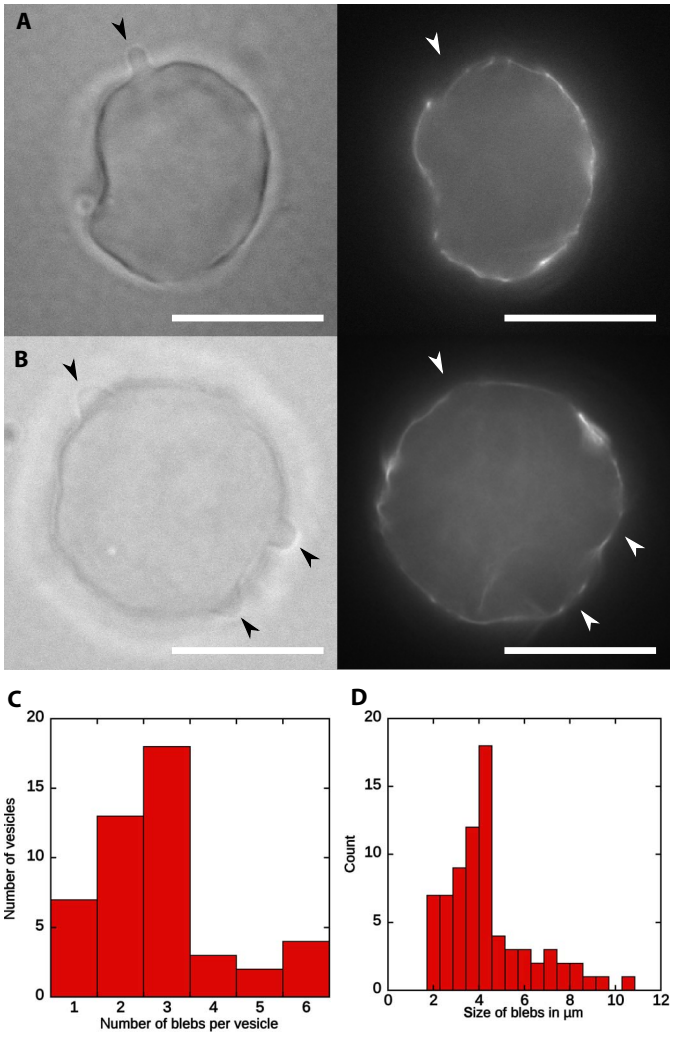

Fig. 3. Cortex heterogeneities lead to blebbing vesicles with a 2D cortex-like structure. (**A** and **B**) Two examples of blebbing vesicles at high anillin and myosin concentration (1 μM anillin/1 μM myosin; 10% Ni-NTA). Bright-field images are shown on the left, and their corresponding epifluorescence images are shown on the right. Scale bars, 20 μm. (**C**) Distribution of the number of blebs observed per vesicle, for the experimental conditions detailed above. (**D**) Size distribution of the small blebs.

Blebbing of active cytoskeletal vesicles

Upon addition of myosin II filaments to the system, a rich morphology is observed. Blebs appear (Figs. 2 and 3) and the shapes of the vesicles change markedly (Fig. 4). Because of the coupling between the network and the membrane, the network cannot contract freely, but instead is constrained by the membrane being pulled against the liquid volume of the vesicle (Fig. 1A). This process results in the establishment of an excess internal pressure p within the fluid. The internal pressure exerts a pushing force on the membrane that is balanced by a force acting on the links joining the actin network to the membrane. This force f is related to the density of the membrane linker ρ and to internal pressure through the relationship $f \sim p/\rho$, because the resistance to the intracellular pressure is shared between linkers. The typical force necessary to rupture an individual Ni-NTA binding link is on the order of a few piconewtons, as determined by single-molecule experiments (*28*, *29*): Above this critical force f^*, the molecular bonds attaching the actin network to the vesicle membrane will break. When a region of the membrane detaches from the actin network, intracellular pressure can then drive the formation of a bleb by exerting a pushing force on the detached membrane region (Fig. 1A).

At high myosin and intermediate cross-linking protein concentrations (0.2:1, anillin/myosin in micromolar), the actin network spans the whole vesicle, and a big stable bleb appears (Fig. 2A). The large bleb has a radius of curvature of about 15 μm (see fig. S5), and its volume accounts for 10 to 17% of the total vesicle volume. The stable bleb is under tension, as seen by the absence of any visible thermal fluctuations of the membrane (Fig. 2A). Because of the vesicle production method, we are not able to image the dynamics of formation of these big blebs that form within a few minutes. Nevertheless, because blebs result from membrane detachment, the growth phase should depend on the total density of linkers; at lower linker densities, bleb growth would be favored, resulting in larger final bleb sizes. Indeed, slightly decreasing the number of membrane attachment points (0.1:1, anillin/myosin in micromolar) results in the appearance of a bleb that takes up the entire vesicle, a process that lasts for more than 15 min (Fig. 2B). First, global contraction of the actin network results in membrane detachment, producing a single bleb that is under tension (Fig. 2C). Subsequently, the cytoskeletal tension becomes so sufficiently high that it ruptures most membrane attachments, allowing almost complete contraction of the network. Alternatively, localized sliding of the anchoring points could also lead to the observed tension release. While the network collapses, the vesicle recovers its spherical shape, and the membrane starts to fluctuate freely, indicating the release of the cytoskeletal-induced membrane tension (Fig. 2, C to E, and movie S1).

Blebbing due to local heterogeneities in active cytoskeletal vesicles

Upon increasing the anillin concentration to 1 μM, we produce vesicles with a 2D cortex and consequently with a much stronger membrane/cytoskeleton coupling (refer to the phase diagram for interlinker distances). In this regime (1:1, anillin/myosin), the vesicles become strongly deformed and faceted, and present multiple small blebs (Fig. 3) significantly different in nature from the blebs observed in the volume-spanning network case. Here, blebbing is a local effect occurring as a result of local heterogeneities in the cortex. We observed one to six blebs having radii of about 2 μm per vesicle (Fig. 3, C and D) and occupying about 0.4 to 2.5% of the total vesicle volume. Thereby, the local position of bleb formation correlates with the local concentration of membrane attachments, which can indeed be observed by the inhomogeneous distribution of the fluorescence intensity of the actin filaments at the circumference of the vesicles (Fig. 3, A and B). The bleb size distribution (Fig. 3D), which spans from 2 to 6 μm, correlates nicely with the size of the regions of low fluorescence intensity previously characterized (Fig. 1G).

After a further increase of anillin (1.5:1), blebbing is then completely inhibited (Fig. 5D), as the sizes of regions with a low actin concentration are effectively lowered (~0.5 μm) (Fig. 1J). Thus, even locally, myosin forces are insufficient to lead to a rupture of the anchoring points of the cortex.

Shape deformation of active cytoskeletal vesicles

At a lower myosin concentration (0.5 μM) (Fig. 4), we observe no more blebbing. Here, the myosin-produced intravesicle pressure decreases,

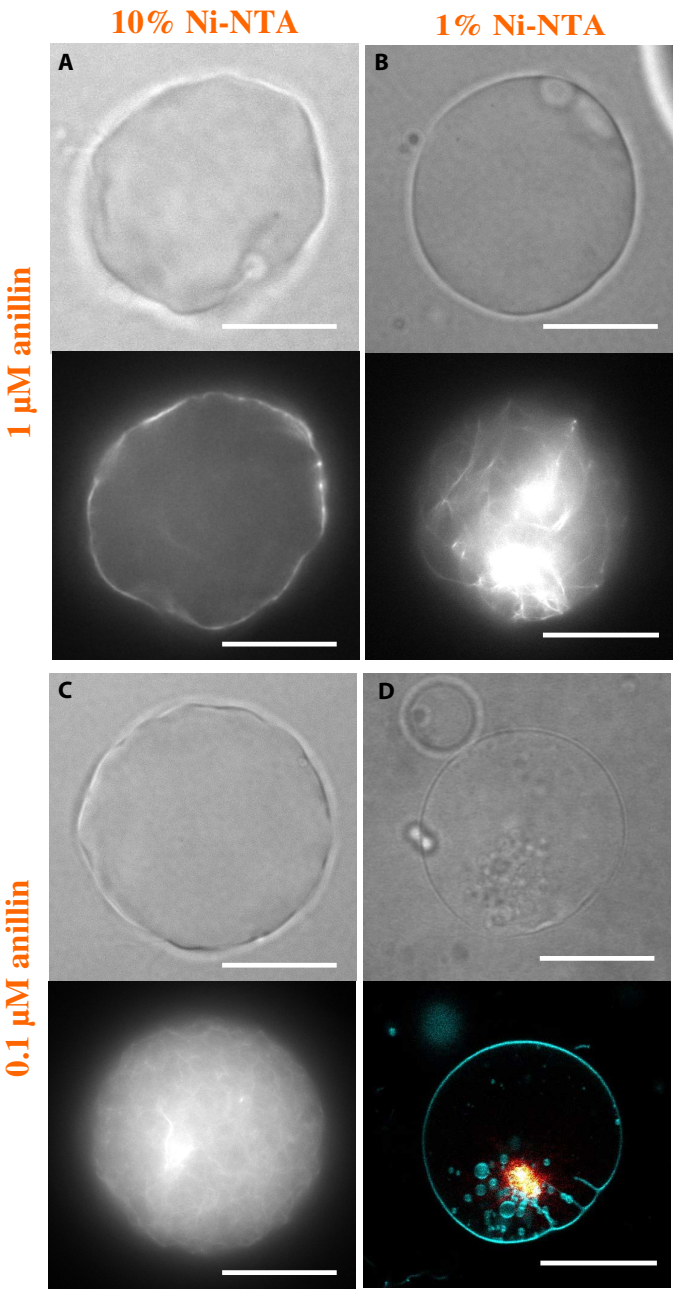

Fig. 4. Morphologies of active vesicles containing 0.5 μM myosin. (**A**) Faceted vesicle with a 2D cortex. (**B**) Decreasing the amount of Ni-NTA lipids in the membrane down to 1% leads to the collapse of the 2D cortex. (**C**) At low anillin concentrations, faceted vesicles contain a 3D network. (**D**) At a lower Ni-NTA percentage, while contracting, the actomyosin extrudes tethers inward the vesicle. The membrane is labeled with 0.1% Texas Red 1,2-dihexadecanoyl-*sn*-glycero-3-phosphoethanolamine, triethylammonium salt (DHPE) lipid. Vesicles are imaged in bright field and epifluorescence in (A) to (C). A confocal image at the equatorial plane is presented in (D). Scale bars, 20 μm.

and is now too small to break the links between the network and the membrane. However, in the vesicles containing a volume-spanning network, stresses generated in the network are sufficient to induce visible deformations in the vesicle contour, resulting in small deformation of vesicles (Fig. 4). While increasing the anillin concentration in the vesicle (1 μM), the network becomes cortex-like, myosin forces induce stronger deformations of the vesicle, and faceted vesicles are observed. Although the measured average circularity of the two vesicle types differs only slightly, the width of the distributions is significantly different (see fig. S6). Stresses within the cortex seem to be more effective in producing highly faceted vesicles, because elastic deformations of the cortex occur more easily than when a volume-spanning network is present. In addition, the bending rigidity of bundles parallel to the membrane in the 2D cortex might resist strongly bending deformations when the vesicle membrane is firmly attached to the network. We never observed these faceted vesicles in cytoskeletal-free or passive cytoskeletal vesicles. Nonspherical shapes can only be produced by internal cytoskeletal tensions, and are dominated by myosin-driven tension and the shear elasticity of the network, rather than by the curvature minimization required by membrane elasticity.

Tethering and vesicularization in active cytoskeletal vesicles

We now note that a range of parameters should exist where the force exerted by the actin network on linkers is too low for the linkers to detach, that is, $f < f^*$, but high enough to deform the lipid membrane to extrude a tether inside the vesicle, $f > f_{tube}$, with f_{tube} being the force needed to pull a membrane tube; $f_{tube} = 2\pi\sqrt{2\kappa\gamma}$ (*30*), with γ being the membrane tension and κ (roughly 20 k_BT) being the bending stiffness of the membrane. For small enough linker densities (3D volume-spanning network) and for an intermediate range of myosin-induced pressures, the actin network should contract by pulling tubes. Indeed, we found that by decreasing the coupling to the membrane by lowering the percentage of Ni-NTA in the membrane to 1% (anillin/myosin concentration, 0.1:0.5), the myosin-generated tensions are sufficient to produce tether formation and vesicularization inside the vesicle (Fig. 4D). This shape transformation is reminiscent of structures observed inside cells, albeit a more specific mechanism of active transport seems to play an important role in living cells (*31*, *32*).

DISCUSSION

To summarize the findings, we mapped the observed dependencies and transitions into a phase diagram (Fig. 5). By precisely controlling the absolute concentrations of all intravesicle components, we establish that the intricate force balance inside a finite volume leads to the complex, arrested, and stable membrane shapes of active cytoskeletal vesicles reminiscent of structures found in living cells. Despite the presence of myosin motors, all observed structures were static and the shape of the deformed vesicles remained stable over several hours. Contrary to living cells, treadmilling of cross-linked actin filaments is an extremely slow process, even in the presence of cofilin (*33*–*35*). The lack of actin turnover prevents the formation of a new contractile actin cortex in the bleb and, in turn, its retraction, as reported for living cells (*36*). The structures that we have built and describe here differ fundamentally from previously described conventional equilibrium structures of pure lipid vesicles, as ours are dominated by the shear elasticity and plastic deformations of an active actin network. Our model system also produced

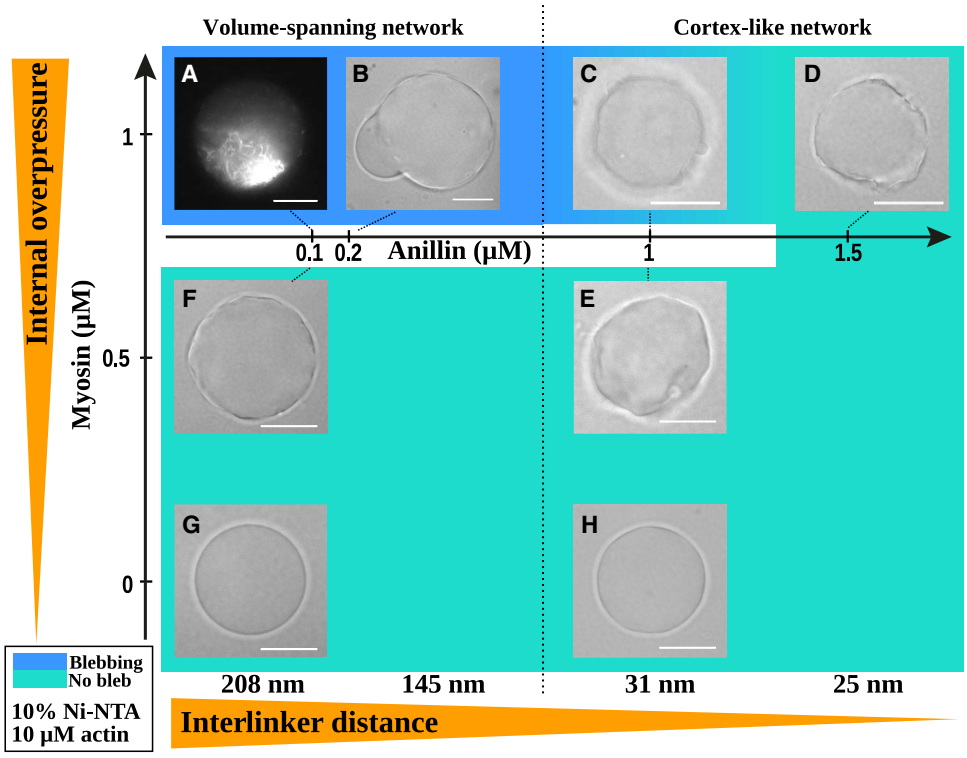

Fig. 5. Experimental phase diagram. (**A** and **B**) Internal overpressure from the actomyosin contraction results in blebs, once it overcomes the membrane/cytoskeleton binding force. We observe this regime for a myosin concentration of 1 μM and an anillin concentration lower than 1 μM. At 1 μm anillin (**C**), blebbing results from local heterogeneities of actin/membrane anchoring in the cortex. Blebbing can be inhibited either by increasing the density of membrane/cytoskeleton linkers [transition from (C) to (**D**)] or by lowering the myosin concentration to 0.5 μM [transition from (A) to (**F**) and from (C) to (**E**)]. Yet, the stress generated by the myosin contraction is strong enough to deform the vesicles. (**G** and **H**) In the absence of myosin, the vesicles remain spherical. Each experimental point results from three to five independent experiments, with up to 60 vesicles. Corresponding fluorescent images of the actin networks can be found in fig. S7. Interlinker distances are summarized in table S1. Scale bars, 20 μm.

the important finding that, for blebbing to occur, the tension generation mechanism must be tightly coupled to the lipid membrane, an organization that is achieved by the membrane having a sufficiently high density of anchoring points. Although the membrane surface tension sets the spherical shape of blebs, our work shows that the active deformability and the shear elasticity of the cytoskeletal network dominate the production of global shape changes in cytoskeletal vesicles. Our bottom-up approach successfully produced active vesicles in vitro that exhibit global shape remodeling driven by the myosin contractile activity. This opens up a completely new avenue for the design of more sophisticated biomimetic systems integrating, for example, actin turnover mechanism or by using proteins from the ERM family to anchor the cytoskeleton to the membrane. This would allow the mimicking of more complex biological processes and the elucidation of the underlying mechanisms that govern them.

MATERIALS AND METHODS

Reagents

Egg L-α-phosphatidylcholine (Egg PC) lipids were ordered from Sigma (P3556) in powder form and dissolved at 50 mg/ml in a chloroform/methanol mixture (9:1, v/v). 1,2-Dipalmitoyl-*sn*-glycero-3-phosphoethanolamine-*N*-[methoxy(polyethylene glycol)-2000] (PEG2000 PE) and 1,2-dioleoyl-*sn*-glycero-3-[(*N*-(5-amino-1-carboxypentyl)iminodiacetic acid)succinyl] (nickel salt) lipids (Ni-NTA) were ordered from Avanti Polar Lipids and dissolved in chloroform. The fluorescent lipid Texas Red DHPE was from Thermo Fisher Scientific. The mineral oil was from Sigma-Aldrich (M3516) and the silicone oil (viscosity, 50 cSt) was from Roth (no. 4020.1). Decane was from Sigma-Aldrich (no. D901).

Proteins

Proteins were purified according to previously published protocols (*37*). G-actin and muscle myosin II were from rabbit skeletal muscle. The fragment of *Xenopus laevis* anillin spanning amino acids 1 to 428, excluding the myosin binding site, was cloned into a pET-28a vector and purified from *Escherichia coli*, with His tags on both termini. To quantify the fraction of anillin at the membrane and in bulk, we labeled it according to the following protocol: we dialyzed it against the labeling buffer [10 mM tris (pH 7.4), 150 mM NaCl, 2 mM EDTA (pH 9), and 2 mM tris(2-carboxyethyl)phosphine]; then, we incubated it with an eightfold excess of Alexa Fluor 488 C_5-maleimide (Molecular Probes) for 2 hours at 4°C and dialyzed it back to the anillin buffer.

Buffer solutions

We mixed the solution to be encapsulated on ice right before vesicle production. Anillin, myosin II, and G-actin were added to a polymerization buffer (pH 7.2). The chemical composition of the solution

(including salts from protein buffers) consisted of 10 mM imidazole, 1 mM $MgCl_2$, 1 mM adenosine triphosphate (ATP), 1 mM EGTA, 30 mM KCl, 2 mM dithiothreitol, 300 mM sucrose, 0.5 μM Alexa Fluor 488 phalloidin, and ATP regenerating system [20 mM creatine phosphate and creatine phosphokinase (0.1 mg/ml)]. The outside solution was made of glucose, whose osmotic pressure was adjusted 10 to 15 mosmol higher than the inside solution.

Preparation of the lipid-in-oil solution

Lipids were dissolved according to a previously published protocol (*26*) that we modified to be able to encapsulate proteins. Lipids dissolved in chloroform and Egg PC lipids dissolved in chloroform/methanol (9:1, v/v) were dispersed into a mineral oil/silicone oil mixture according to the following protocol. In a 20-ml glass vial, lipids were added to 600 μl of decane. Then, 9.4 ml of the mineral oil/silicone oil mixture was added to the lipids/decane solution while gently vortexing. The resulting lipid concentration was 0.5 mM and the oil composition consisted of 80% silicone oil and 20% (mineral oil + initial decane).

Vesicle production

Vesicles were produced using the cDICE method described by Abkarian *et al.* (*25*). Briefly, it consisted of a cylindrical rotating chamber, successively filled with a glucose solution to collect the vesicles, a lipid-in-oil solution to saturate the oil/water (O/W) interfaces, and decane as the continuous phase in which droplets were produced. The solution containing the cytoskeletal elements was injected from a glass capillary by inserting the capillary's tip in the decane. Because of the centrifugal force, droplets detached from the tip. The droplets then moved through the lipid-in-oil solution where they were coated by a first lipid monolayer and then by a second lipid monolayer while crossing the O/W interface. The two monolayers zipped together to form a bilayer. Vesicles were collected in the glucose solution, which was sucked with a micropipette once the chamber was stopped. For the process to succeed, the osmolarity of the encapsulated solution has to match that of the glucose solution. The membrane was doped with 2.5% of PEG2000 PE to prevent nonspecific protein adsorption. The whole process was achieved in a cold room maintained at 5°C to prevent fast polymerization of the cytoskeleton. We produced vesicles in a span of 2 min, which allowed us to have the sample on the microscope 5 to 7 min after protein mixing. During this time, the actin already polymerized and the final state of the vesicles was reached, which prevented us from imaging the initiation of bleb formation or shape changes. Although cDICE is a high-yield method, resulting in hundreds of vesicles under most conditions, encapsulating proteins at high concentrations (10 μm of actin and up to 1 μm of anillin and myosin) resulted in a decrease of the yield. At the highest protein concentrations we reported here, a 100-μl sample contained about 50 vesicles.

Microscopy

Vesicles were imaged with a Leica Microscope DMI3000 B and a 63× numerical aperture (N.A.) 1.3 oil immersion objective for bright-field microscopy and epifluorescence, in combination with a Hamamatsu ORCA-ER camera. Confocal pictures were acquired with a Leica TSC SP5 and a 63× N.A. 1.4 oil immersion objective.

SUPPLEMENTARY MATERIALS

Supplementary material for this article is available at http://advances.sciencemag.org/cgi/content/full/2/4/e1500465/DC1

Shape analysis of faceted vesicles
His-anillin binding to the actin network and to the membrane
Estimates of binding affinities
Membrane/network bound anillin
table S1. Calculated bound anilin concentration under different conditions.
fig. S1. Actin network in vesicles in the absence of Ni-NTA lipids.
fig. S2. Different contributions of anillin.
fig. S3. Controls of membrane functionalization and encapsulation.
fig. S4. Determination of the ratio of cortical anillin.
fig. S5. Size distribution of the big stable blebs.
fig. S6. Circularity of faceted vesicles containing 0.5 μM myosin.
fig. S7. Phase diagram with fluorescent images.
movie S1. Fluctuations of the lipid membrane before and after complete actomyosin contraction.
References (*38*–*40*)

REFERENCES AND NOTES

1. C. Le Clainche, M.-F. Carlier, Regulation of actin assembly associated with protrusion and adhesion in cell migration. *Physiol. Rev.* **88**, 489–513 (2008).
2. T. Lecuit, P.-F. Lenne, E. Munro, Force generation, transmission, and integration during cell and tissue morphogenesis. *Annu. Rev. Cell Dev. Biol.* **27**, 157–184 (2011).
3. G. Charras, E. Paluch, Blebs lead the way: How to migrate without lamellipodia. *Nat. Rev. Mol. Cell Biol.* **9**, 730–736 (2008).
4. H.-G. Döbereiner, E. Evans, M. Kraus, U. Seifert, M. Wortis, Mapping vesicle shapes into the phase diagram: A comparison of experiment and theory. *Phys. Rev. E* **55**, 4458–4474 (1997).
5. K. Berndl, J. Käs, R. Lipowsky, E. Sackmann, U. Seifert, Shape transformations of giant vesicles: Extreme sensitivity to bilayer asymmetry. *Europhys. Lett.* **13**, 659 (1990).
6. Y. Li, H. Kusumaatmaja, R. Lipowsky, R. Dimova, Wetting-induced budding of vesicles in contact with several aqueous phases. *J. Phys. Chem. B* **116**, 1819–1823 (2012).
7. S. Köhler, V. Schaller, A. R. Bausch, Structure formation in active networks. *Nat. Mater.* **10**, 462–468 (2011).
8. M. P. Murrell, M. L. Gardel, F-actin buckling coordinates contractility and severing in a biomimetic actomyosin cortex. *Proc. Natl. Acad. Sci. U.S.A.* **109**, 20820–20825 (2012).
9. A.-C. Reymann, R. Boujemaa-Paterski, J.-L. Martiel, C. Guérin, W. Cao, H. F. Chin, E. M. De La Cruz, M. Théry, L. Blanchoin, Actin network architecture can determine myosin motor activity. *Science* **336**, 1310–1314 (2012).
10. F. C. Keber, E. Loiseau, T. Sanchez, S. J. DeCamp, L. Giomi, M. J. Bowick, M. C. Marchetti, Z. Dogic, A. R. Bausch, Topology and dynamics of active nematic vesicles. *Science* **345**, 1135–1139 (2014).
11. D. Merkle, N. Kahya, P. Schwille, Reconstitution and anchoring of cytoskeleton inside giant unilamellar vesicles. *ChemBioChem* **9**, 2673–2681 (2008).
12. M. Murrell, L.-L. Pontani, K. Guevorkian, D. Cuvelier, P. Nassoy, C. Sykes, Spreading dynamics of biomimetic actin cortices. *Curr. Biol.* **100**, 1400–1409 (2011).
13. F.-C. Tsai, B. Stuhrmann, G. H. Koenderink, Encapsulation of active cytoskeletal protein networks in cell-sized liposomes. *Langmuir* **27**, 10061–10071 (2011).
14. L.-L. Pontani, J. van der Gucht, G. Salbreux, J. Heuvingh, J.-F. Joanny, C. Sykes, Reconstitution of an actin cortex inside a liposome. *Biophys. J.* **96**, 192–198 (2009).
15. K. Carvalho, F.-C. Tsai, E. Lees, R. Voituriez, G. H. Koenderink, C. Sykes, Cell-sized liposomes reveal how actomyosin cortical tension drives shape change. *Proc. Natl. Acad. Sci. U.S.A.* **110**, 16456–16461 (2013).
16. A. D. Lieber, S. Yehudai-Resheff, E. L. Barnhart, J. A. Theriot, K. Keren, Membrane tension in rapidly moving cells is determined by cytoskeletal forces. *Curr. Biol.* **23**, 1409–1417 (2013).
17. M. Dogterom, G. Koenderink, Cell-membrane mechanics: Vesicles in and tubes out. *Nat. Mater.* **10**, 561–562 (2011).
18. A. Clark, O. Wartlick, G. Salbreux, E. K. Paluch, Stresses at the cell surface during animal cell morphogenesis. *Curr. Biol.* **24**, R484–R494 (2014).
19. E. Paluch, C.-P. Heisenberg, Biology and physics of cell shape changes in development. *Curr. Biol.* **19**, R790–R799 (2009).
20. V. Ruprecht, S. Wieser, A. Callan-Jones, M. Smutny, H. Morita, K. Sako, V. Barone, M. Ritsch-Marte, M. Sixt, R. Voituriez, C.-P. Heisenberg, Cortical contractility triggers a stochastic switch to fast amoeboid cell motility. *Cell* **160**, 673–685 (2015).
21. Y.-J. Liu, M. Le Berre, F. Lautenschlaeger, P. Maiuri, A. Callan-Jones, M. Heuzé, T. Takaki, R. Voituriez, M. Piel, Confinement and low adhesion induce fast amoeboid migration of slow mesenchymal cells. *Cell* **160**, 659–672 (2015).
22. G. Salbreux, G. Charras, E. Paluch, Actin cortex mechanics and cellular morphogenesis. *Trends Cell Biol.* **22**, 536–545 (2012).
23. J.-Y. Tinevez, U. Schulze, G. Salbreux, J. Roensch, J.-F. Joanny, E. Paluch, Role of cortical tension in bleb growth. *Proc. Natl. Acad. Sci. U.S.A.* **106**, 18581–18586 (2009).
24. A. R. Bausch, K. Kroy, A bottom-up approach to cell mechanics. *Nat. Phys.* **2**, 231–238 (2006).

25. M. Abkarian, E. Loiseau, G. Massiera, Continuous droplet interface crossing encapsulation (cDICE) for high throughput monodisperse vesicle design. *Soft Matter* **7**, 4610–4614 (2011).
26. C. Claudet, M. In, G. Massiera, Method to disperse lipids as aggregates in oil for bilayers production. *Eur. Phys. J. E Soft Matter Biol. Phys.* **39**, 9 (2016).
27. J. Liu, G. D. Fairn, D. F. Ceccarelli, F. Sicheri, A. Wilde, Cleavage furrow organization requires PIP_2-mediated recruitment of anillin. *Curr. Biol.* **22**, 64–69 (2012).
28. R. Merkel, P. Nassoy, A. Leung, K. Ritchie, E. Evans, Energy landscapes of receptor ligand bonds explored with dynamic force spectroscopy. *Nature* **397**, 50–53 (1999).
29. C. Verbelen, H. J. Gruber, Y. F. Dufrłne, The NTA–His_6 bond is strong enough for AFM single-molecular recognition studies. *J. Mol. Recognit.* **20**, 490–494 (2007).
30. I. Derényi, F. Jülicher, J. Prost, Formation and interaction of membrane tubes. *Phys. Rev. Lett.* **88**, 238101 (2002).
31. C. G. Almeida, A. Yamada, D. Tenza, D. Louvard, G. Raposo, E. Coudrier, Myosin 1b promotes the formation of post-Golgi carriers by regulating actin assembly and membrane remodelling at the *trans*-golgi network. *Nat. Cell Biol.* **13**, 779–789 (2011).
32. S. Miserey-Lenkei, G. Chalancon, S. Bardin, E. Formstecher, B. Goud, A. Echard, Rab and actomyosin-dependent fission of transport vesicles at the Golgi complex. *Nat. Cell Biol.* **12**, 645–654 (2010).
33. K. M. Schmoller, C. Semmrich, A. R. Bausch, Slow down of actin depolymerization by cross-linking molecules. *J. Struct. Biol.* **173**, 350–357 (2011).
34. D. Breitsprecher, S. A. Koestler, I. Chizhov, M. Nemethova, J. Mueller, B. L. Goode, J. V. Small, K. Rottner, J. Faix, Cofilin cooperates with fascin to disassemble filopodial actin filaments. *J. Cell Sci.* **124**, 3305–3318 (2011).
35. E. De La Cruz, How cofilin severs an actin filament. *Biophys. Rev.* **1**, 51–59 (2009).
36. G. T. Charras, C.-K. Hu, M. Coughlin, T. J. Mitchison, Reassembly of contractile actin cortex in cell blebs. *J. Cell Biol.* **175**, 477–490 (2006).
37. S. Köhler, K. M. Schmoller, A. H. Crevenna, A. R. Bausch, Regulating contractility of the actomyosin cytoskeleton by pH. *Cell Rep.* **2**, 433–439 (2012).
38. S. Suzuki, K. Abe, Topological structural analysis of digitized binary images by border following. *Comput. Vision Graphics Image Process.* **30**, 32–46 (1985).
39. A. Weins, J. S. Schlondorff, F. Nakamura, B. M. Denker, J. H. Hartwig, T. P. Stossel, M. R. Pollak, Disease-associated mutant α-actinin-4 reveals a mechanism for regulating its F-actin-binding affinity. *Proc. Natl. Acad. Sci. U.S.A.* **104**, 16080–16085 (2007).
40. O. Lieleg, M. M. A. E. Claessens, A. R. Bausch, Structure and dynamics of cross-linked actin networks. *Soft Matter* **6**, 218–225 (2010).

Acknowledgments

Funding: Research was supported by ERC-SelfOrg (European Research Council–Self Organization in Cytoskeletal Systems) (E.L., F.C.K., and A.R.B.) and partly by the SFB863 and the Nanosystems Initiative Munich (E.L., F.C.K., and A.R.B.). A.R.B. acknowledges the hospitality of the Miller Institute for Basic Research in Science at the University of Berkeley. **Author contributions:** E.L., G.S., and A.R.B. planned the experiment. J.A.M.S. and G.S. developed the theoretical model; E.L., F.C.K., and C.P. performed the experiments; E.L. and A.R.B. performed data analysis; G.M. provided important insights into the vesicle formation process; and E.L., J.A.M.S., G.S., and A.R.B. wrote the paper. **Competing interests:** The authors declare that they have no competing interests. **Data and materials availability:** All data needed to evaluate the conclusions in the paper are present in the paper and/or the Supplementary Materials. Additional data related to this paper may be requested from the authors.

Submitted 13 April 2015
Accepted 22 March 2016
Published 15 April 2016
10.1126/sciadv.1500465

Citation: E. Loiseau, J. A. M. Schneider, F. C. Keber, C. Pelzl, G. Massiera, G. Salbreux, A. R. Bausch, Shape remodeling and blebbing of active cytoskeletal vesicles. *Sci. Adv.* **2**, e1500465 (2016).

Shape remodeling and blebbing of active cytoskeletal vesicles

Etienne Loiseau, Jochen A. M. Schneider, Felix C. Keber, Carina Pelzl, Gladys Massiera, Guillaume Salbreux and Andreas R. Bausch

Sci Adv **2** (4), e1500465.
DOI: 10.1126/sciadv.1500465